Spin excitation spectrum in striped bilayer compounds

Frank Krüger and Stefan Scheidl
Institut für Theoretische Physik, Universität zu Köln, Zülpicher Str. 77, D-50937 Köln, Germany
(Received 19 January 2004; published 30 August 2004)

The spin dynamics of bilayer cuprate compounds are studied in a basic model. The magnetic spectral properties are calculated in linear spin-wave theory for several stripe configurations which differ by the relative location of the stripes in the layers. We focus on the bilayer splitting of the magnon bands near the incommensurate low energy peaks as well as near the π resonance, distinguishing between the odd and even channel. We find that an x-shaped dispersion near the π resonance is generic for stripes. By comparison of our results to neutron scattering data for $YBa_2Cu_3O_{6+x}$ we conclude that the stripe model is consistent with characteristic features of bilayer high-T_c compounds.

DOI: 10.1103/PhysRevB.70.064421 PACS number(s): 75.10.Jm, 74.72.−h, 75.30.Ds, 76.50.+g

I. INTRODUCTION

Subsequent to predictions of stripe formation,[1–3] characteristic signatures of spin and charge order have been found in a variety of high-T_c cuprate superconductors, including $La_{2-x}Sr_xCuO_4$ (LSCO) and $YBa_2Cu_3O_{6+x}$ (YBCO). Neutron scattering experiments[4,5] have provided evidence for spin order at low energies through a pattern of incommensurate peaks around the antiferromagnetic wave vector. Although more difficult to detect, charge order has been observed in LSCO codoped with Nd (Ref. 6) as well as in YBCO without codoping.[7]

Since LSCO and YBCO are paradigmatic for monolayer and bilayer compounds, stripelike "low"-energy response is characteristic for both classes of materials. On the other hand, at "high" energies spin fluctuations appeared to be qualitatively different since a commensurate π resonance had been observed only in bilayer compounds, notably in $YBa_2Cu_3O_{6+x}$ (Refs. 8 and 9) and $Bi_2Sr_2CaCu_2O_{8+x}$,[10] whereas it seemed to be absent in monolayer compounds. This apparent distinction between monolayer and bilayer compounds lost its justification only recently, when the π resonance was discovered in $Tl_2Ba_2CuO_{6+x}$ (Ref. 11) as the first monolayer compound. The fact that the π-resonant mode has not been detected in LSCO so far can possibly be ascribed to a larger effective strength of disorder, since the Sr dopants are randomly distributed whereas in the oxygen doped compounds the access oxygen orders in chains. Thus, one may believe that, in principle, monolayer and bilayer compounds have qualitatively similar features also at higher energies. This universality of low- and high-energy features calls for an even more unifying framework.[12]

In a recent article[13] we have analyzed an elementary monolayer model assuming that charges form a perfectly ordered site-centered stripe array which imposes a static spatial modulation of spin-exchange couplings. The resulting spin dynamics was studied using linear spin-wave theory. As a result, we found that the incommensurability and the π resonance appear as complementary features of the band structure at different energy scales. Furthermore, the doping dependence of the resonance frequency was found in good agreement with experimental observations.

In this work we extend this model to bilayer systems in order to predict the corresponding features of the magnon band structure and the magnetic structure factor. Within each layer, holes are assumed to form unidirectional site-centered stripes. We consider several possibilities (parallel and perpendicular relative orientations) of the charge order in the antiferromagnetically coupled neighboring layers. The band structure and the $T=0$ inelastic structure factor for even and odd excitations are calculated in linear spin-wave theory. Particular attention is paid to the band splitting in the vicinity of the antiferromagnetic wave vector and to the influence of the interlayer coupling on the π-resonance energy.

The outline of this paper is as follows. In Sec. II the spin-only model for a bilayer system is introduced and motivated. Classical ground states and the resulting phase diagrams for competing types of magnetic order are obtained. They are needed as a starting point for the linear spin-wave theory. A customized formulation thereof is outlined in Sec. III. The results, namely the spin-wave band structure, the zero-temperature structure factor for even and odd excitations, and the dependence of the band splitting at the antiferromagnetic wave vector on the strength of the interlayer coupling are presented in Sec. IV and compared to experiments in Sec. V.

II. MODEL

Stripes are a combined charge- and spin-density wave. If the charge period pa is a multiple of the Cu spacing a with integer p, lock-in effects tend to suppress phasonlike fluctuations of the density modulation. In a reductionist real-space picture, one may think of the holes forming parallel site-centered rivers of width a, which act as antiphase domain boundaries for the antiferromagnetic spin domains in between.[6] This implies that the period of the spin modulation is twice that of the charge modulation.

To implement that the charge stripes act like antiphase boundaries we follow our previous work[13] and choose the simplest possible implementation of exchange couplings within the layers stabilizing this magnetic structure: antiferromagnetic exchange couplings J between neighboring spins within the domains and antiferromagnetic couplings λJ between closest spins across a stripe.

In our previous work[13] we have studied this model for a single layer allowing for diagonal and vertical stripe orienta-

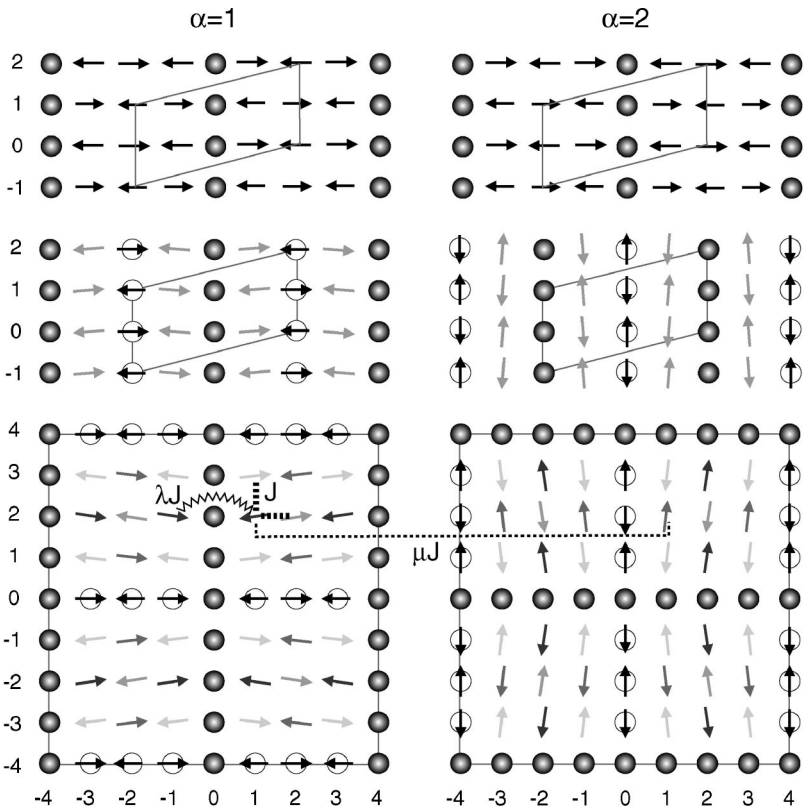

FIG. 1. Classical ground states for bilayer systems with parallel (upper row), shifted parallel (middle row), and perpendicular hole stripes (lower row) for a stripe spacing $p=4$. The exchange couplings of the simple model are illustrated in the lower row: AF couplings $J>0$ for nearest neighbors within the domains (bold dashed), λJ between nearest neighbors across a hole stripe (zig-zag) and couplings μJ between spins one above the other (dashed). Frustration of exchange coupling may lead to a canting of spins (calculated for $\mu=0.09$ and $\lambda=0.07$ in the middle and bottom row, respectively). Possible magnetic unit cells are outlined by gray lines, identical gray levels of spins correspond to identical canting angles.

tions. Here we focus on vertical stripes as observed in the superconducting cuprates and restrict our analysis to the representative case $p=4$. This corresponds to a doping of one hole per eight Cu sites since the rivers have a line charge of only half a hole per lattice constant. In addition to the in-plane couplings we consider an antiferromagnetic exchange μJ between two layers (cf. Fig. 1). The Hamiltonian of this bilayer model is given by

$$H=\sum_{\alpha=1,2} H_\alpha + H_{1,2}, \tag{1a}$$

$$H_\alpha=\frac{1}{2}\sum_{\mathbf{r},\mathbf{r}'}^{*} J_\alpha(\mathbf{r},\mathbf{r}')\mathbf{S}_\alpha(\mathbf{r})\mathbf{S}_\alpha(\mathbf{r}'), \tag{1b}$$

$$H_{1,2}=\mu J\sum_{\mathbf{r}}^{*}\mathbf{S}_1(\mathbf{r})\mathbf{S}_2(\mathbf{r}), \tag{1c}$$

where $\mathbf{r}$ specifies the square-lattice position and $\alpha=1,2$ numbers the layers. The asterisks indicate that the sums do not include positions of charge rivers. The in-plane couplings $J_\alpha(\mathbf{r},\mathbf{r}')$ defined in the text above are illustrated in Fig. 1. They explicitly depend on the layer index if the charge distribution is different in both layers.

For simplicity we neglect spin anisotropy, the weak three-dimensional coupling between bilayers, and more complicated exchange processes such as cyclic exchange or Dzyaloshinskii-Moriya interactions, which all may be important for quantitative purposes. Obviously, this simple spin-only model does not account for electronic correlation effects, e.g., a spin gap at low energies due to the formation of Cooper pairs is not incorporated. Nevertheless we expect that our model provides a qualitatively adequate description of the spin fluctuations well above the gap energy.

The actual stripe configuration is determined by several influences. Besides the magnetic exchange energy one must also take into account the Coulomb energy, and in principle also a further reduction of the fourfold symmetry of CuO_2 planes in orthorhombic structures which may favor a certain alignment of the stripes. In $YBa_2Cu_3O_{6+x}$ the formation of CuO chains along the *b* direction may favor a parallel alignment of stripes.

We find that three different stripe configurations may be realized physically (see Fig. 1). The exchange energy favors *parallel stripes* lying exactly on top of each other. This configuration is free of magnetic exchange frustration, each bond can be fully saturated. However, this configuration is disfavored by the Coulomb energy which would favor a configuration where stripes are *parallel but shifted* with respect to each other by half a stripe spacing. (In our simple model, where holes are assumed to be site centered, this configuration is only compatible with even stripe spacings *p*.) The gain in Coulomb energy must be paid by a loss of exchange energy. For certain parameters, a third configuration may be favorable, where the charge stripes of the two layers are *perpendicular*.

For the latter analysis it is instructive to anticipate that for these configurations the Hamiltonian has discrete symmetries. We focus on symmetries involving an exchange of layers. For parallel and shifted parallel stripes, this symmetry is just the reflection $z\rightarrow -z$ combined with a translation (coordinates are chosen such that the planes are parallel to the *xy* plane). For perpendicular stripes, one needs to add a rotation around the *z* axis.

A. Energetic estimates

To estimate the Coulomb energy for the three stripe configurations, we assume a charge-density modulation $\rho(\mathbf{r}) = \rho_1(\mathbf{r})\delta(z) + \rho_2(\mathbf{r})\delta(z-d)$ with $\rho_\alpha(\mathbf{r}) = \rho_\alpha^{(0)}\cos(\mathbf{k}_\alpha \mathbf{r})$ where the planes separated by d are perpendicular to the z direction. For simplicity, only the first harmonic of the charge modulation is retained. Parallel stripes are described by $\mathbf{k}_1 = \mathbf{k}_2 = k\mathbf{e}_x$ and $\rho_1^{(0)} = \rho_2^{(0)} = \overline{\rho}$, shifted parallel stripes are realized for $\mathbf{k}_1 = \mathbf{k}_2 = k\mathbf{e}_x$ and $\rho_1^{(0)} = -\rho_2^{(0)} = \overline{\rho}$, and perpendicular stripes for $\mathbf{k}_1 = k\mathbf{e}_x$, $\mathbf{k}_2 = k\mathbf{e}_y$ and $\rho_1^{(0)} = \rho_2^{(0)} = \overline{\rho}$. For a stripe spacing pa the charge-modulation wave vectors are given by $k = 2\pi/(pa)$, the amplitude by $\overline{\rho} = e/(2pa^2)$. Calculating the Coulomb coupling energy per square lattice site

$$E_C = \frac{1}{4\pi\epsilon_0}\frac{a^2}{A}\int \mathrm{d}^3 r \int \mathrm{d}^3 r' \frac{\rho_1(\mathbf{r})\rho_2(\mathbf{r}')}{|\mathbf{r}-\mathbf{r}'|}, \tag{2}$$

where A denotes the area of the planes, we find, in the limit $A \to \infty$, a vanishing Coulomb coupling for perpendicular stripes, an energy cost

$$\Delta E_C = \frac{e^2}{32\pi\epsilon_0 pa}\exp\left(-2\pi\frac{d}{pa}\right) \tag{3}$$

for parallel stripes, and an energy gain of the same size for shifted parallel stripes. For YBCO with $a \approx 3.85$ Å, $d \approx 3.34$ Å, $J = 125$ meV, $S = \frac{1}{2}$ and for a stripe spacing $p = 4$ we obtain $\Delta E_C \approx 29$ meV.

For antiferromagnetic YBCO the magnetic interlayer superexchange is reported to be $\mu \approx 0.08$.[14] For parallel stripes, spins are not frustrated and, in a classical picture, antiparallel in different layers, $\mathbf{S}_1(\mathbf{r}) = -\mathbf{S}_2(\mathbf{r})$. Thus, the exchange coupling roughly leads to an energy gain of order $\mu J S^2 \approx 3$ meV, whereas the energy gain will be smaller for the other two configurations due to frustration.

Thus, within our rough estimate, the Coulomb energy appears to be up to one order of magnitude larger than the exchange energy, such that one might expect the parallel shifted configuration to be the only physical one. On the other hand, the actual Coulomb energy may be significantly smaller than the result of our estimate since we have completely neglected screening. For almost undoped YBCO a relative large value of $\epsilon \approx 15$ for the static dielectric constant at $T = 4$ K is reported.[15] Therefore the Coulomb energy might be of the same order of magnitude as the magnetic exchange energy. Because of the crudeness of our estimate no stripe configuration can be strictly ruled out.

B. Classical ground states

Due to frustration effects, the ground-state structure is nontrivial for shifted parallel and perpendicular stripes. We now determine these ground states treating spins as classical. These ground states will be a necessary prerequisite for the subsequent spin-wave analysis. We continue to focus on the representative case $p = 4$.

Depending on the values of the couplings λ and μ we find two different types of ground states. For a nearest neighbor exchange across a stripe in the range $0 < \lambda < \lambda_c$ ($\lambda_c \approx 0.59$ for shifted parallel and $\lambda_c \approx 0.35$ for perpendicular stripes) the ground state has a canted planar topology up to a value $\mu_c(\lambda)$ of the interlayer exchange (cf. Fig. 2). For $\mu > \mu_c(\lambda)$ spins lock into a collinear texture.

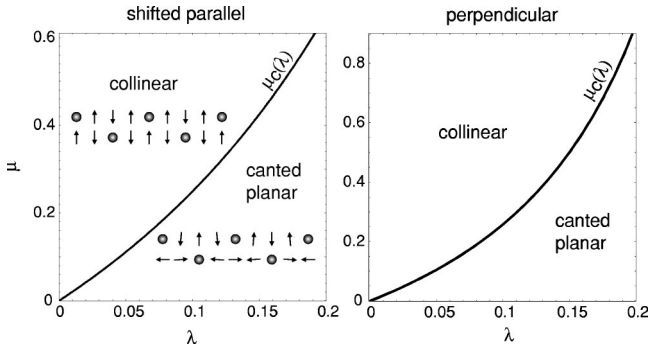

FIG. 2. Classical ground-state phase diagrams for shifted parallel and perpendicular stripes. For $\mu < \mu_c(\lambda)$ the ground states show a canted planar spin pattern illustrated in Fig. 1. For $\mu > \mu_c(\lambda)$ the topology of the ground states changes into a collinear pattern where spins lying on top of each other are strictly antiparallel and nearest neighbors across a stripe are parallel. For $\lambda \to \lambda_c$ ($\lambda_c \approx 0.59$ for shifted parallel and $\lambda_c \approx 0.35$ for perpendicular stripes) μ_c goes to infinity. Above λ_c the ground states are always planar.

To characterize these different phases, we start with the planar one. As already indicated above, the frustration can lead to a canting of spins. The origin of the canting is easily understood. For $\mu = 0$ the layers are decoupled and the sublattice magnetization in both layers can have an arbitrary relative orientation. For small interlayer coupling μ the spins start to cant starting from a configuration where spins lying on top of each other are perpendicular. Only in this case the interlayer couplings lead to an energy gain proportional to small canting angles while the intralayer couplings lead to an energy cost of second order in the canting angles. Such canted planar ground states are illustrated in Fig. 1. In Fig. 3 the corresponding tilting angles are plotted for $\lambda = 0.1$ as a function of μ. The tilting angles increase monotonously in a way that spins lying on top of each other become increasingly antiparallel with increasing μ.

In the other phase, for $\mu > \mu_c(\lambda)$, the interlayer coupling μ dominates the coupling λ across the stripes and the topology of the ground state changes into a collinear configuration where the spins lying on top of each other are strictly antiparallel and nearest neighbor spins across a stripe are strictly parallel although they are antiferromagnetically coupled. This configuration is stable against a canting of the spins because for small λ the energy gain for λ bonds and the energy costs for μ bonds as well as the couplings within the domains would be quadratic in the tilting angles. Since this ground state has lost the antiphase-boundary character of the charge stripes it resembles a diluted antiferromagnet. This would lead to a static magnetic response at the antiferromagnetic wave vector in disagreement with experimental observations. Therefore, these collinear phases probably are not relevant for the magnetic properties of the cuprate compounds.

For small values of λ the phase boundary is approximately given by $\mu_c(\lambda) \approx 2\lambda$ for both stripe configurations

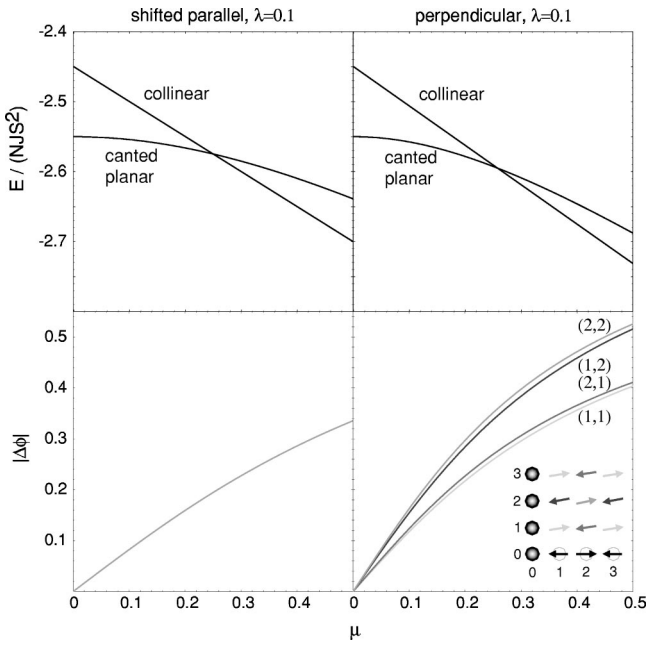

FIG. 3. Upper row: Energy per lattice site in units of JS^2 as a function of μ for $\lambda=0.1$. For both stripe configurations the energies of the canted planar and the collinear spin pattern are plotted. The curves intersect at $\mu=\mu_c$ where the topology of the ground states changes. Lower row: Relative values of the tilting angles of the spins in the planar configuration as a function of the interlayer coupling μ for $\lambda=0.1$.

(cf. Fig. 2). In the limit $\lambda\to\lambda_c$ the critical value μ_c goes to infinity. Above λ_c the ground states remain canted planar for all values of the interlayer coupling μ.

Comparing the classical magnetic ground-state energies for the two frustrated configurations, we find that—in contrast to the Coulomb energy — the exchange coupling favors perpendicular stripes over shifted parallel stripes. For this reason we retain perpendicular stripes in our consideration.

III. SPIN-WAVE THEORY

In this analytic part we derive general expressions for the magnon band structure and the spectral weight at zero temperature in a framework of linear spin-wave theory (for a review in the context of cuprates, see e.g., Ref. 16). These expressions are evaluated numerically later on in Sec. IV for parallel, shifted parallel, and perpendicular stripes and fixed stripe spacing $p=4$.

A. Holstein-Primakoff representation

The ground-state analysis of the preceding section has made clear that spin waves now have to be introduced as excitation of a noncollinear ground state. However, our numerical calculations of the classical ground states have shown planar spin textures (here, a collinear texture is considered as a special subcase of a planar texture).

In the following we consider a general planar ground state which can be captured by a vector field $\mathbf{S}_\alpha(\mathbf{r})=\{\cos\phi_\alpha(\mathbf{r}),\sin\phi_\alpha(\mathbf{r}),0\}$, where the tilting angles of the spins obey the translational symmetry $\phi_\alpha(\mathbf{r})=\phi_\alpha(\mathbf{r}+\mathbf{A})$ for an arbitrary magnetic lattice vector $\mathbf{A}=m_1\mathbf{A}^{(1)}+m_2\mathbf{A}^{(2)}$. For the spin textures displayed in Fig. 1, corresponding magnetic unit cells are given by $\mathbf{A}^{(1)}=(4,1)$ and $\mathbf{A}^{(2)}=(0,2)$ for parallel stripes and for shifted parallel stripes, and by $\mathbf{A}^{(1)}=(8,0)$ and $\mathbf{A}^{(2)}=(0,8)$ for perpendicular stripes.

To study the quantum fluctuation around the classical ground state we rotate all spins by their planar angles $\phi_\alpha(\mathbf{r})$ according to

$$S^x_\alpha(\mathbf{r})=\tilde{S}^x_\alpha(\mathbf{r})\cos\,\phi_\alpha(\mathbf{r})-\tilde{S}^y_\alpha(\mathbf{r})\sin\,\phi_\alpha(\mathbf{r}), \tag{4a}$$

$$S^y_\alpha(\mathbf{r})=\tilde{S}^x_\alpha(\mathbf{r})\sin\,\phi_\alpha(\mathbf{r})+\tilde{S}^y_\alpha(\mathbf{r})\cos\,\phi_\alpha(\mathbf{r}), \tag{4b}$$

$$S^z_\alpha(\mathbf{r})=\tilde{S}^z_\alpha(\mathbf{r}), \tag{4c}$$

such that $\tilde{\mathbf{S}}(\mathbf{r})$ has a classical ferromagnetic ground state $\tilde{\mathbf{S}}(\mathbf{r})=S\{1,0,0\}$. In the transformed spin basis we introduce Holstein-Primakoff (HP) bosons in the standard way (using $\tilde{S}^\pm=\tilde{S}^y\pm i\tilde{S}^z$),

$$\tilde{S}^+_\alpha(\mathbf{r})=\sqrt{2S-\hat{n}_{\mathbf{r},\alpha}}\,b_{\mathbf{r},\alpha}, \tag{5a}$$

$$\tilde{S}^-_\alpha(\mathbf{r})=b^\dagger_{\mathbf{r},\alpha}\sqrt{2S-\hat{n}_{\mathbf{r},\alpha}}, \tag{5b}$$

$$\tilde{S}^x_\alpha(\mathbf{r})=-\hat{n}_{\mathbf{r},\alpha}+S, \tag{5c}$$

and obtain the spin-wave Hamiltonian

$$\mathcal{H}=\frac{S}{2}\sum_{\mathbf{r},\mathbf{r}'}^{*}\sum_{\alpha,\alpha'}\{f_{\alpha,\alpha'}(\mathbf{r},\mathbf{r}')[b^\dagger_{\mathbf{r}\alpha}b_{\mathbf{r}'\alpha'}+b_{\mathbf{r}\alpha}b^\dagger_{\mathbf{r}'\alpha'}] + g_{\alpha,\alpha'}(\mathbf{r},\mathbf{r}')[b_{\mathbf{r}\alpha}b_{\mathbf{r}'\alpha'}+b^\dagger_{\mathbf{r}\alpha}b^\dagger_{\mathbf{r}'\alpha'}]\}, \tag{6}$$

where the functions f and g are defined by

$$f_{\alpha,\alpha'}(\mathbf{r},\mathbf{r}')=\frac{1}{2}[J_\alpha(\mathbf{r},\mathbf{r}')\delta_{\alpha,\alpha'}+\mu J\delta_{\mathbf{r},\mathbf{r}'}(1-\delta_{\alpha,\alpha'})]\times[\Delta_{\alpha,\alpha'}(\mathbf{r},\mathbf{r}')+1] - \delta_{\mathbf{r},\mathbf{r}'}\delta_{\alpha,\alpha'}\sum_{\mathbf{r}''}J_\alpha(\mathbf{r},\mathbf{r}'')\Delta_{\alpha,\alpha}(\mathbf{r},\mathbf{r}'') - \mu J\delta_{\mathbf{r},\mathbf{r}'}\delta_{\alpha,\alpha'}\sum_{\alpha''}(1-\delta_{\alpha,\alpha''})\Delta_{\alpha,\alpha''}(\mathbf{r},\mathbf{r}), \tag{7a}$$

$$g_{\alpha,\alpha'}(\mathbf{r},\mathbf{r}')=\tfrac{1}{2}[J_\alpha(\mathbf{r},\mathbf{r}')\delta_{\alpha,\alpha'}+\mu J\delta_{\mathbf{r},\mathbf{r}'}(1-\delta_{\alpha,\alpha'})]\times[\Delta_{\alpha,\alpha'}(\mathbf{r},\mathbf{r}')-1], \tag{7b}$$

$$\Delta_{\alpha,\alpha'}(\mathbf{r},\mathbf{r}')=\cos[\phi_\alpha(\mathbf{r})-\phi_{\alpha'}(\mathbf{r}')]. \tag{7c}$$

To diagonalize the Hamiltonian, we Fourier transform the bosonic operators via $b_\alpha(\mathbf{r})=\int_{\mathbf{k}}\exp(i\mathbf{kr})b_\alpha(\mathbf{k})$, where $\int_{\mathbf{k}}=(2\pi)^{-2}\int d^2k$ and the $\mathbf{k}$ integrals run over the Brillouin zone of the square lattice with an area $(2\pi/a)^2$. Following our calculations for the monolayer system[13] we decompose a

square lattice vector $\mathbf{r}$ into a magnetic lattice vector $\mathbf{A}$ and a decoration vector $\mathbf{a}$ ($\mathbf{r}=\mathbf{A}+\mathbf{a}$). The number of vectors $\mathbf{a}$ is denoted by n (the area of the magnetic unit cell). In momentum space, the reciprocal magnetic basis $\mathbf{Q}^{(i)}$, $i=1,2$, spans the corresponding magnetic Brillouin zone ($\mathcal{BZ}$). Wave vectors $\mathbf{k}$ can be uniquely decomposed into $\mathbf{k}=\mathbf{Q}+\mathbf{q}$ with $\mathbf{q}\in\mathcal{BZ}$ and $\mathbf{Q}=m_1\mathbf{Q}^{(1)}+m_2\mathbf{Q}^{(2)}$. Within the Brillouin zone of the square lattice there are n vectors $\mathbf{Q}$ which we denote by $\mathbf{Q}_\nu$. Using these decompositions we rewrite the spin-wave Hamiltonian as

$$\mathcal{H}=\frac{1}{2}\int_{\mathbf{q}}\sum_{\nu,\nu'}\sum_{\alpha,\alpha'}F_{\nu\alpha,\nu'\alpha'}(\mathbf{q})[b^\dagger_{\alpha,\mathbf{q}+\mathbf{Q}_\nu}b_{\alpha',\mathbf{q}+\mathbf{Q}_{\nu'}}+b_{\alpha,-\mathbf{q}-\mathbf{Q}_\nu}b^\dagger_{\alpha',-\mathbf{q}-\mathbf{Q}_{\nu'}}]+\frac{1}{2}\int_{\mathbf{q}}\sum_{\nu,\nu'}\sum_{\alpha,\alpha'}G_{\nu\alpha,\nu'\alpha'}(\mathbf{q})\times[b^\dagger_{\alpha,\mathbf{q}+\mathbf{Q}_\nu}b^\dagger_{\alpha',-\mathbf{q}-\mathbf{Q}_{\nu'}}+b_{\alpha,-\mathbf{q}-\mathbf{Q}_\nu}b_{\alpha',\mathbf{q}+\mathbf{Q}_{\nu'}}], \tag{8}$$

where

$$F_{\nu\alpha,\nu'\alpha'}(\mathbf{q})=\frac{S}{n}\sum_{\mathbf{A}}\sum_{\mathbf{a},\mathbf{a}'}f_{\alpha,\alpha'}(\mathbf{a}+\mathbf{A},\mathbf{a}')\times\cos[\mathbf{q}\mathbf{A}+\mathbf{q}(\mathbf{a}-\mathbf{a}')+\mathbf{Q}_\nu\mathbf{a}-\mathbf{Q}_{\nu'}\mathbf{a}'] \tag{9}$$

is essentially the Fourier transform of f,

$$\frac{S}{n}f_{\alpha,\alpha'}(\mathbf{Q}_\nu+\mathbf{q},\mathbf{Q}_{\nu'}+\mathbf{q}')=\delta(\mathbf{q}+\mathbf{q}')F_{\nu\alpha,\nu'\alpha'}(\mathbf{q}). \tag{10}$$

Analogous expressions relate G to g. The Hamiltonian (8) has exactly the same structure as in the monolayer case [compare Eq. (8) in Ref. 13] and can be diagonalized by a Bogoliubov transformation in an analogous way. The final diagonal form is given by

$$\mathcal{H}=\sum_{\gamma=1}^{2n}\int_{\mathbf{q}}\omega_\gamma(\mathbf{q})\{b^\dagger_\gamma(\mathbf{q})b_\gamma(\mathbf{q})+\tfrac{1}{2}\}, \tag{11}$$

where the squared energies ω_γ^2 are eigenvalues of the Hermitian matrix $\mathbf{M}^{-1/2}\mathbf{K}\mathbf{M}^{-1/2}$. Thereby $\mathbf{M}^{-1}=\mathbf{F}-\mathbf{G}$ denotes the inverse mass matrix and $\mathbf{K}=\mathbf{F}+\mathbf{G}$ the coupling matrix.

B. Structure factor

We now proceed to calculate the inelastic zero-temperature structure factor for even and odd excitations

$$\mathcal{S}^{\mathrm{in}}_\pm(\mathbf{k},\omega):=\sum_{\mathbf{F}}\sum_{j=x,y,z}|\langle\mathrm{F}|S^j_1(\mathbf{k})\pm S^j_2(\mathbf{k})|0\rangle|^2\delta(\omega-\omega_\mathrm{F}). \tag{12}$$

Here, $|0\rangle$ denotes the ground state (magnon vacuum) characterized by $b_\gamma(\mathbf{q})|0\rangle=0$ and we consider only single-magnon final states $|\mathrm{F}\rangle=b^\dagger_\gamma(\mathbf{q})|0\rangle$ with excitation energy $\omega_\mathrm{F}:=E_\mathrm{F}-E_0$. $\mathbf{k}=(k_x,k_y)$ denotes the in-plane wave vector, odd excitations correspond to $k_z^-=(2n+1)\pi/d$ [$L^-=(2n+1)c/(2d)$ in reciprocal lattice units], even ones to $k_z^+=2n\pi/d$ ($L^+=nc/d$), where d is the distance of the two layers within the orthorhombic unit cell. For YBCO with $d\approx3.34$ Å and $c\approx11.7$ Å the corresponding values for even and odd modes are $L^-\approx1.75,5.25$ and $L^+\approx0,3.5$.

Expressing the spin operators by the final bosonic operators $b_\gamma(\mathbf{q})$ it is straightforward to calculate the structure factor. Using a pseudo-Dirac notation and denoting the $2n$-dimensional Cartesian basis by $|\nu,\alpha\rangle\rangle$ ($\nu=1,\ldots,N,\alpha=1,2$) and the orthonormal eigenbasis of $\mathbf{M}^{-1/2}\mathbf{K}\mathbf{M}^{-1/2}$ by $|\gamma\rangle\rangle$, the structure factor can be rewritten in a compact form,

$$\mathcal{S}^{\mathrm{in}}_\pm(\mathbf{q}+\mathbf{Q}_\nu,\omega)=S\sum_\gamma\mathcal{S}^\pm_\gamma(\mathbf{q}+\mathbf{Q}_\nu)\delta(\omega-\omega_\gamma(\mathbf{q})), \tag{13a}$$

$$\mathcal{S}^\pm_\gamma(\mathbf{q}+\mathbf{Q}_\nu)=\frac{1}{2}\sum_{\mathbf{X}=\mathbf{C},\mathbf{S},\omega_\gamma^{-1}\mathbf{K}}\langle\langle\nu,\pm|\mathbf{X}\mathbf{M}^{-1/2}|\gamma\rangle\rangle\times\frac{1}{\omega_\gamma}\langle\langle\gamma|\mathbf{M}^{-1/2}\mathbf{X}|\nu,\pm\rangle\rangle, \tag{13b}$$

where we have defined $|\nu,\pm\rangle\rangle=(1/\sqrt{2})[|\nu,1\rangle\rangle\pm|\nu,2\rangle\rangle]$ and introduced the matrices $\mathbf{S}$ and $\mathbf{C}$ according to

$$s_{\nu\alpha,\nu'\alpha'}=\frac{1}{n}\delta_{\alpha\alpha'}\sum_{\mathbf{a}}^{*}\sin\,\phi_\alpha(\mathbf{a})e^{i(\mathbf{Q}_\nu-\mathbf{Q}_{\nu'})\mathbf{a}}, \tag{14a}$$

$$c_{\nu\alpha,\nu'\alpha'}=\frac{1}{n}\delta_{\alpha\alpha'}\sum_{\mathbf{a}}^{*}\cos\,\phi_\alpha(\mathbf{a})e^{i(\mathbf{Q}_\nu-\mathbf{Q}_{\nu'})\mathbf{a}}. \tag{14b}$$

IV. RESULTS

We now evaluate the magnon dispersion and the inelastic structure factor for even and odd excitations numerically. From a comparison of our findings for the monolayer system to neutron scattering data for the cuprate compounds we found[13] the coupling λJ across a stripe to be about one order of magnitude smaller than the nearest neighbor coupling J within the domains. For the coupling μJ between the layers a value $\mu\approx0.08$ is reported[14] for antiferromagnetic YBCO in the absence of stripes. Therefore in the stripe system the couplings λ and μ can be assumed to be of the same order. In the following we keep the value of λ fixed and discuss the effects of increasing μ starting from the case of decoupled layers ($\mu=0$) where the band structure of the monolayer system[13] should be recovered. In this parameter regime the classical ground states for shifted parallel and perpendicular charge stripes show the canted planar texture and the antiphase domain boundary character of the charge stripe is weakened by the interlayer coupling but still pronounced. Finally we shortly present the excitation spectra for shifted parallel and perpendicular stripes for parameters belonging to the collinear ground state regime.

In the case of decoupled layers ($\mu=0$) the results of the monolayer system are trivially recovered. Since the two layers are uncorrelated, the structure factor does not depend on the L component of the wave vector. For parallel stripes (with or without a relative shift of the stripes) where the charge modulation is unidirectional with $\mathbf{Q}_1^{\mathrm{ch}}=\mathbf{Q}_2^{\mathrm{ch}}=(1/4,0)$ we just obtain an additional twofold degeneracy of each of

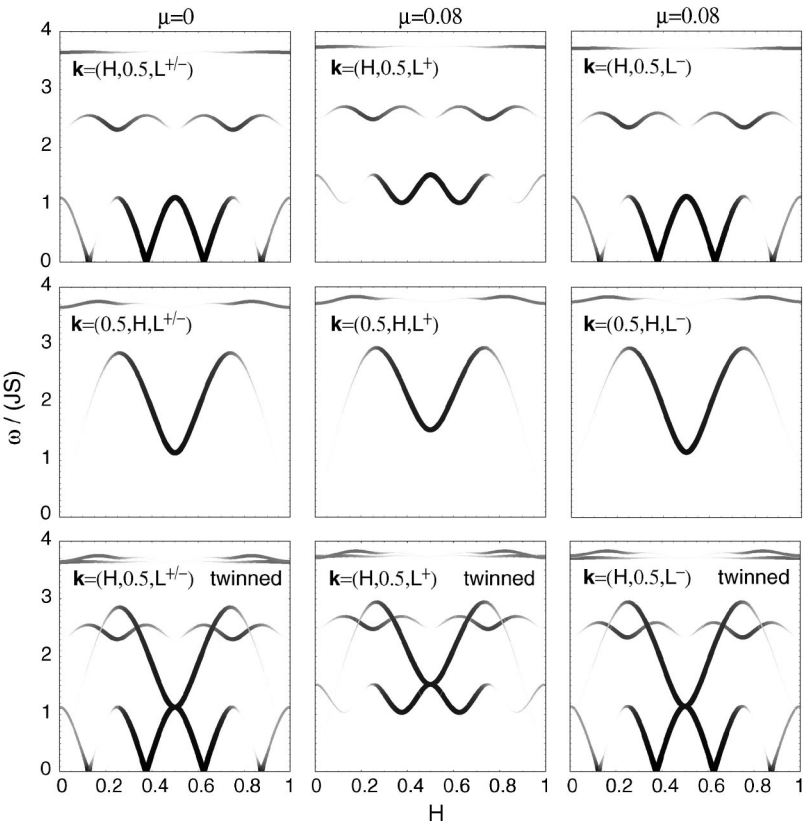

FIG. 4. Band structure and spectral weight along the $(H,0.5,L^{\pm})$ and $(0.5,H,L^{\pm})$ directions for parallel stripes lying on top of each other and couplings $\lambda=0.15$ and $\mu=0,0.08$. The last row shows the band structure of a twinned sample (see text). L^{+} corresponds to even, L^{-} to odd excitations. Darker and larger points correspond to a larger weight of the inelastic structure factor.

the three bands due to the equivalence of the two layers. Therefore the degeneration of the bands is fourfold since in the monolayer case each band is twofold degenerated due to the equivalence of the two sublattices.[13] The lowest, acoustical band has zeros at the magnetic superstructure vectors which are located at $(j/4,0)$ and $(j/4+1/8,1/2)$, $j=0,\ldots,3$, within the Brillouin zone of the square lattice (we choose $0\leqslant H,K<1$). The spectral weight is concentrated near the lowest harmonic incommensurate wave vectors $\mathbf{Q}=(1/2\pm1/8,1/2)$. With increasing energy the incommensurability decreases and the branches of the acoustic magnon band close at the antiferromagnetic wave vector $(1/2,1/2)$ and an energy ω_{π} which we associate with the π resonance. Along the $(H,1/2)$ direction the acoustic band is gapped to the overlying optical magnon band (see upper left panels in Figs. 4 and 5). Along the orthogonal direction $(1/2,K)$, one optical band has vanishing spectral weight and only two bands are visible (see middle-left panels in Figs. 4 and 5).

In twinned samples with stripe domains oriented orthogonal to each other, a scan along the $(H,1/2)$ direction results in the superposition of the signals obtained from scans in directions $(H,1/2)$ and $(1/2,H)$ of a single-domain sample. For domains of equal size, one thus obtains an apparent symmetry $(H,K)\leftrightarrow(K,H)$ and a fourfold pattern of the static incommensurate wave vectors located at $\mathbf{Q}=(1/2\pm1/8,1/2)$ and $\mathbf{Q}=(1/2,1/2\pm1/8)$ also for (shifted) parallel stripes. In Figs. 4 and 5, the panels in the third row are just obtained by superimposing the panels of the first and second row. Since the acoustic band of the monolayer system has a saddle point at the antiferromagnetic wave vector, the resulting band structure is x-shaped in the vicinity of the π-resonance energy.

The configuration of hole stripes lying perpendicular to each other corresponds to charge modulation wave vectors $\mathbf{Q}_1^{\mathrm{ch}}=(1/4,0)$ and $\mathbf{Q}_2^{\mathrm{ch}}=(0,1/4)$. For decoupled layers, the resulting band structure contains the bands of the monolayer system and the same bands rotated by 90 degrees leading to the symmetry $\omega(H,K)=\omega(K,H)$ and therefore to a fourfold pattern of the static incommensurate wave vectors located at $\mathbf{Q}=(1/2\pm1/8,1/2)$ and $\mathbf{Q}=(1/2,1/2\pm1/8)$. Thus, for $\mu=0$, the structure factor is identical for perpendicular stripes and twinned parallel stripes (left lower panel in Figs. 4 and 5).

With increasing interlayer coupling μ the bands start to split with different distributions of the spectral weights in the odd and even channel (cf. Figs. 4–6). For parallel and shifted parallel stripes the Hamiltonian is invariant under the reflection $z\rightarrow -z$ combined with a translation. This implies that the magnon states—modulo a phase factor which does not enter the structure factor — have a well-defined parity with respect to an exchange of both layers. As a consequence, nondegenerate bands are visible only either in the even or the odd channel.

Nevertheless the excitation spectra of the two parallel stripe configurations deviate significantly, e.g., the even excitations are gapped for parallel stripes whereas for shifted parallel stripes the intensity of even excitations is only reduced at low energies (cf. middle columns of Figs. 4 and 5). For stripes on top of each other, each band — which is fourfold degenerate at $\mu=0$ — splits up into twofold degenerate bands which have identical parity. For shifted stripes each band splits up into three bands. One of them is twofold degenerate and both subbands are of opposite parity. Therefore this degenerated band is visible in both channels (cf. Fig. 5).

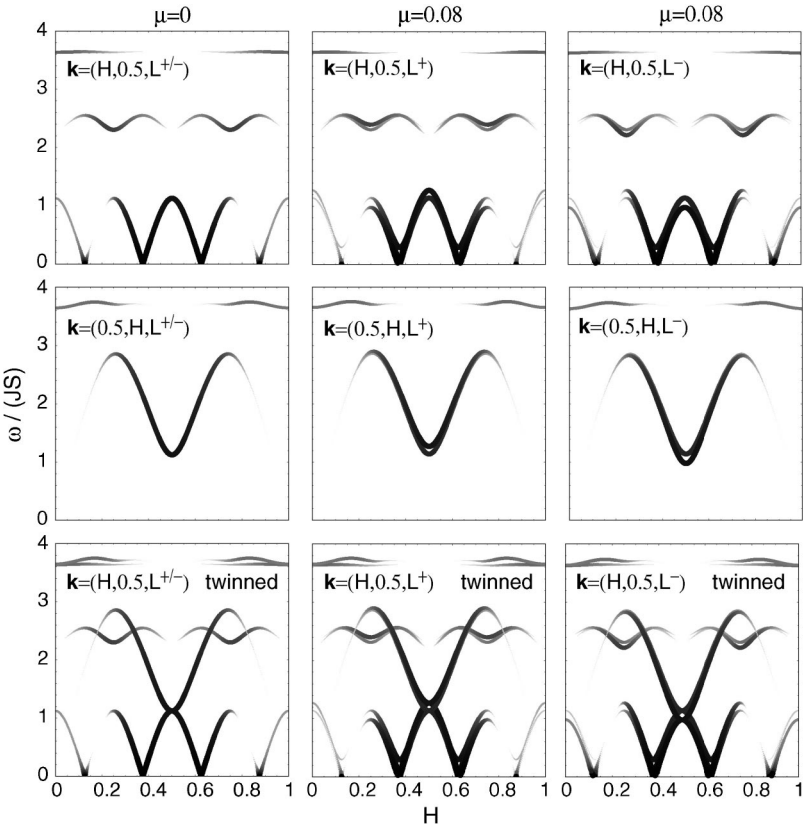

FIG. 5. Band structure and spectral weight along the $(H,0.5,L^{\pm})$ and $(0.5,H,L^{\pm})$ directions for shifted parallel stripes and couplings $\lambda=0.15$ and $\mu=0,0.08$. The last row shows the resulting band structure of a twinned sample.

For perpendicular stripes the symmetry is more complicated. The Hamiltonian is invariant under a reflection $z\rightarrow -z$ in combination with a 90° rotation along the z axis. Since this rotation mixes different wave vectors, almost all eigenstates do not have a well-defined parity and will be partially visible in the odd and even channel. The exception are modes at particular wave vectors such as the antiferromagnetic wave vector which are mapped onto themselves (modulo a reciprocal lattice vector). Only there the excitations can be classified due to their symmetry. Like for the shifted parallel stripes the excitations are not gapped in the even channel (cf. Fig. 6).

We now focus on the band splitting and the distribution of the spectral weights of even and odd excitations at the antiferromagnetic wave vector $(1/2,1/2)$. With increasing interlayer coupling μ, the resonance energy ω_π splits up into two different energies ω_π^- and ω_π^+ for centered-parallel stripes and into three energies ω_π^-, ω_π^0, and ω_π^+ for the other stripe configurations as schematically illustrated in Fig. 7. It is common to all stripe configurations that ω_π^- has a finite spectral weight only in the odd channel, whereas ω_π^+ has a finite weight only in the even channel. For shifted parallel and perpendicular stripes, in both channels a finite intensity is found at the intermediate energy ω_π^0. This intensity is however smaller than at $\omega_\pi^\pm$.

The splitting of the resonance energy for shifted parallel and perpendicular stripes looks quite similar. ω_π^- and ω_π^+ are almost equidistant to the intermediate energy ω_π^0 which increases only slightly with μ (cf. Fig. 8). For small couplings the splitting is quadratic in μ. For centered-parallel stripes the splitting looks different, ω_π^+ increases almost linearly with μ whereas ω_π^- is almost independent of the interlayer coupling.

Finally, we calculate the band structures for shifted parallel and perpendicular stripes for couplings $\lambda<\lambda_c$ and $\mu>\mu_c(\lambda)$ where the ground states are collinear and the

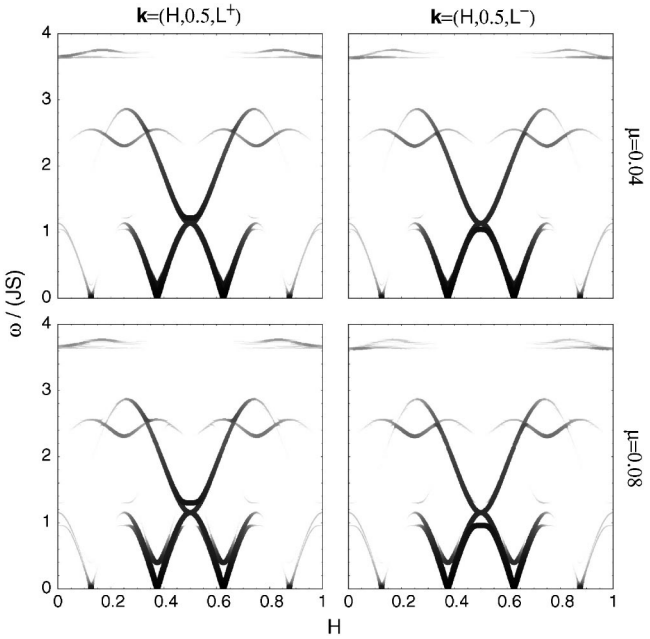

FIG. 6. Band structure and spectral weight for even (left panel) and odd (right panel) excitations along $(H,0.5,L^{\pm})$ direction for perpendicular stripes with couplings $\lambda=0.15$ across the stripes and interlayer couplings $\mu=0.04$ (upper row) and $\mu=0.08$ (lower row).

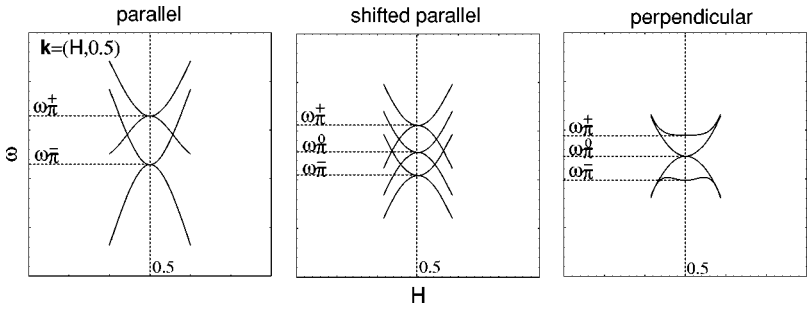

FIG. 7. Schematic illustration of the band splitting in the vicinity of the antiferromagnetic wave vector $(1/2,1/2)$ along the $(H,1/2)$ direction. In the cases of parallel stripes the band structures for twinned samples are shown. Even and odd bands are gathered together.

charge stripes lose their antiphase domain boundary character. We implicitly assume that μ is not too large, otherwise spins on top of each other dimerize and lose their magnetization. In this regime the magnetic fluctuations are drastically changed. For both stripe orientations, the odd channel now has a static signal at the antiferromagnetic wave vector, whereas in the even channel the spectral weight is concentrated at incommensurate position $(1/2\pm1/4,1/2)$ (cf. Fig. 9). For perpendicular stripes we also find small intensity at this position in the odd channel. The incommensurability is doubled compared to the regime of canted planar ground states reflecting that the charge stripes do not act like antiphase domain boundaries in the regime of strongly coupled layers. In the even channel the intensity at the antiferromagnetic wave vector is peaked at an energy ω_π which increases with the interlayer coupling μ and is approximately the same for both stripe configurations.

V. DISCUSSION

In this section we compare our results to neutron scattering data for the bilayer high-T_c compound $YBa_2Cu_3O_{6+x}$. We wish to stress that—because of the simplifications assumed in our model—it is not our goal to obtain a quantitative agreement. Rather we wish to draw a qualitative comparison in order to fortify the hypothesis that the stripe picture is a suitable approach to describe spin fluctuations. Furthermore, we hope that a comparison of future experimental data with our calculations will help to identify the realized stripe configuration.

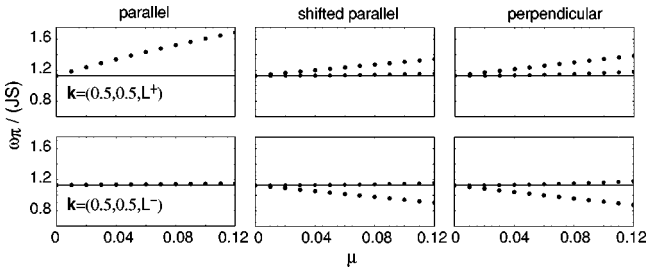

FIG. 8. Splitting of the resonance energy as a function of the interlayer coupling μ for $\lambda=0.15$. In the odd channel $(L=L^-)$ the spectral weight is concentrated at ω_π^- and no intensity is found at ω_π^+, in the even channel $(L=L^+)$ no excitations at ω_π^- are observable and the spectral weight is concentrated at ω_π^+. For shifted and perpendicular stripes in both channels a small intensity is found at the intermediate energy ω_π^0.

Since a spin gap with an energy ω_{gap}—e.g., due to Cooper-pair formation — is not incorporated in our model, the results apply only to energies above ω_{gap} where the magnon dispersion is not masked by the superconducting condensate. In particular in the underdoped regime where ω_{gap} decreases with the doping level, the calculated spectral features become visible over an increasing energy range. Our calculations are restricted to zero temperature. Therefore, a comparison can also be made only to experiments performed at temperatures well below the superconducting transition temperature.

Experiments[17–19] in (partially) detwinned YBCO provide evidence for unidirectional order, i.e., that a fourfold pattern of incommensurate peaks near the antiferromagnetic wave vector $\mathbf{k}_{\mathrm{AF}}=(1/2,1/2)$ results only from the twinning. The stripes seem to be parallel and oriented along the direction of the oxygen chains in the adjacent planes. This immediately speaks against the scenario of perpendicular stripes for which detwinning would not affect the fourfold symmetry.

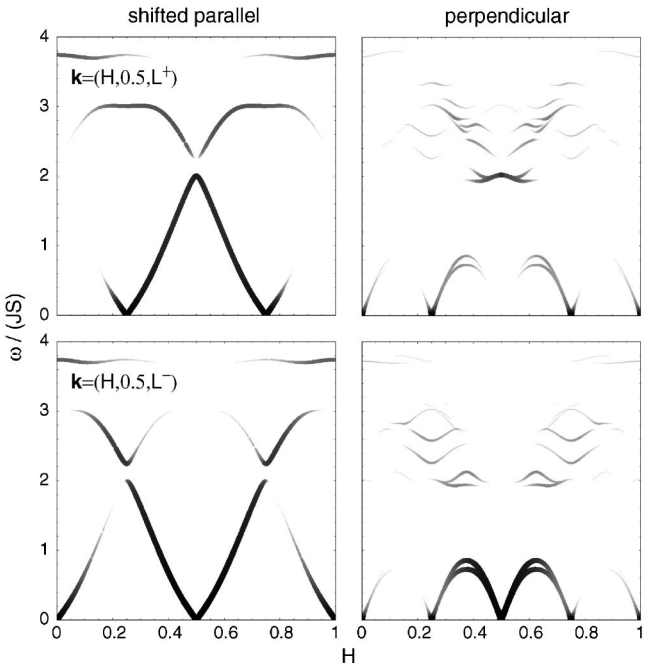

FIG. 9. Band structure in the collinear regime $\mu>\mu_c(\lambda)$ along the direction $(H,1/2,L^\pm)$ for shifted parallel and perpendicular stripes with $\lambda=0.07$ and $\mu=0.50$.

TABLE I. Spin dynamics data for $YBa_2Cu_3O_{6+x}$ for various oxygen concentrations x characterized by the critical temperatures T_c, incommensurability δ, corresponding stripe period p, the resonance energy ω_π^- observed in the odd channel, and ω_π^+.

x	0.35	0.45	0.5	0.5	0.6	0.7	0.7	0.7
T_c (K)	39	48	52	59	63	67	67	74
δ (r.l.u.)	1/16			0.08	0.10	1/8		0.1
p	8			6.25	5	4		5
ω_π^- (meV)	23	30.5	31.5	33	34	36	33	37
ω_π^+ (meV)						41	50	
Ref.	7	23	23	19	23	24	25	23

We briefly recall some neutron scattering measurements on $YBa_2Cu_3O_{6+x}$ which provide insight into the incommensurability and the π resonance over a wide doping and temperature range. It was controversial for quite some time whether both phenomena would exist above T_c until in underdoped materials the incommensurability was found also above T_c.[20] Likewise, the appearance of the magnetic resonance was found above T_c, occurring together with the pseudogap at a temperature $T^* > T_c$ determined from transport and nuclear resonance.[21] Although the π resonance persists as a well-defined feature also in the normal state above T_c, its intensity can be reduced significantly at T_c.[19] For near optimally doped compounds, the resonance is not detectable in the normal phase[22] since T^* almost coincides with T_c. Dai *et al.*[23] concluded that the resonance exists above T_c for $x \leqslant 0.8$ and that incommensurate spin fluctuations appear in the normal state for $x \leqslant 0.6$. Arai *et al.*[24] also observed incommensurate fluctuations in the normal state for a sample with an oxygen concentration of $x=0.7$. Thus, superconductivity is not a prerequisite for incommensurability and π resonance in bilayer compounds as well as in monolayer compounds.

For underdoped YBCO with various oxygen concentrations, the experimentally observed spin dynamics data (see Table I) look qualitatively very similar. There is a systematic increase of the incommensurability and of the π-resonance frequency with doping, which is consistent with our model. We have shown this recently for a monolayer model.[13] The bilayer stripe model shares this feature and therefore we focus in this paper exclusively on specific bilayer features.

Experimentally, constant energy scans slightly above the gap in the odd channel along $(H,1/2,L^-)$ show a broad intensity peak at $\mathbf{k}_{\mathrm{AF}}$, before incommensurate scattering sets in and the data can be compared to our model. The intensity shows magnetic peaks at a distance $\delta k(\omega)$ away from $\mathbf{k}_{\mathrm{AF}}$. The incommensurability δ is determined by extrapolating $\delta k(\omega)$ to $\omega=0$ and it is connected to the stripe spacing p through $\delta=1/(2p)$. The incommensurate peaks are best defined if the stripe spacing is nearly a multiple of the lattice spacing (integer p) since the stripes are stabilized by the lattice.[7]

The three stripe configurations examined for our model are not equivalent in their low-energy behavior. For (unshifted) parallel stripes (see Fig. 4), an incommensurability is visible at low energies only in the odd channel since the even channel has a relatively large gap not related to superconductivity. In contrast, for shifted parallel and perpendicular stripes the even channel shows incommensurate response down to the superconducting gap. Experimental evidence[21,25,26] for a large gap in the even channel (well above the resonance energy in odd channel) therefore favors the configuration with unshifted parallel stripes.

With increasing energy, the separation $\delta k(\omega)$ of the incommensurate peaks decreases and the branches close at $\mathbf{k}_{\mathrm{AF}}$ at certain energies ω_π. Depending on the stripe configuration, there are two or three such energies, compare Fig. 7. According to our model, an energy scan of the odd channel at $\mathbf{k}_{\mathrm{AF}}$ would show a first resonance at the intersection with the lowest magnon band at ω_π^- which we identify with the resonance frequency.[8,27] For shifted parallel and perpendicular stripes, a second line at ω_π^0 contributes to the odd channel. It has significantly less weight and is separated from the first one by only a small energy splitting (of the order of a few meV) which would be hard to be resolved experimentally.

In a similar way, the even channel has a resonance at an energy $\omega_\pi^+ > \omega_\pi^-$, and for shifted parallel and perpendicular stripes also a weaker resonance at an intermediate frequency ω_π^0 (cf. Fig. 7). Experimentally,[19,27,28] a strong oscillatory dependence of the scattering intensity on L shows that the resonance frequencies in the odd and even channel are well separated. Energy scans at the antiferromagnetic wave vector show peaks at ω_π^- in the odd channel and ω_π^+ in the even channel, no peak at the intermediate energy ω_π^0 which should be visible in both channels is resolved.[25] This again favors unshifted parallel stripes, which (in contrast to shifted parallel and perpendicular stripes) have no shared resonance frequency ω_π^0. Although we restricted our comparison to experiments on underdoped samples, overdoped compounds also show two distinct resonance modes of opposite symmetry,[29] which could be identified with ω_π^- and ω_π^+.

From a comparison of the band splitting $\Delta\omega_\pi=\omega_\pi^+-\omega_\pi^-$ to experimental values (cf. Table I) we can estimate the strength of the interlayer coupling μ. For $\lambda=0.15$ we find $\mu \approx 0.02-0.06$ almost independent of the stripe configuration. This value is reasonable since the effective coupling μ in the stripe system should be slightly reduced compared to the undoped case where a value of $\mu \approx 0.08$ is reported.[14]

Above ω_π the response is found to become incommensurate again with increasing separation $\delta k(\omega)$. The momentum width is larger and the intensity is weaker than below ω_π. Overall, the dispersion is "x-shaped." As pointed out in Sec. IV such a shape appears basically for every nonunidirectional stripe configuration, for parallel stripes in twinned crystals as well as in perpendicular stripes. The x-shape has been observed explicitly in Refs. 7 and 24–26. It would be interesting to verify in detwinned samples that the relative intensities of the upper and lower branches of the x-shape are related to the population ratio of the twin domains.

In conclusion, we have calculated the bilayer effects in the magnetic excitation spectrum in striped states. As a generic feature of the stripe model we find an x-shaped dispersion in the vicinity of the π resonance, which is

consistent with experimental data. We have obtained a bilayer splitting of single-layer bands into two or three bilayer bands. From the three stripe configurations studied, the unshifted parallel case overall is most consistent with neutron scattering data, although it seems to be energetically unfavorable at first sight.

ACKNOWLEDGMENTS

We gratefully acknowledge helpful discussions with M. Braden, Y. Sidis, and J. M. Tranquada. This project was supported financially by Deutsche Forschungsgemeinschaft (SFB608).

[1] J. Zaanen and O. Gunnarsson, Phys. Rev. B **40**, 7391 (1989).
[2] H. J. Schulz, J. Phys. (Paris) **50**, 2833 (1989).
[3] K. Machida, Physica C **158**, 192 (1989).
[4] S.-W. Cheong, G. Aeppli, T. E. Mason, H. Mook, S. M. Hayden, P. C. Canfield, Z. Fisk, K. N. Clausen, and J. L. Martinez, Phys. Rev. Lett. **67**, 1791 (1991).
[5] H. A. Mook, P. Dai, S. M. Hayden, G. Aeppli, T. G. Perring, and F. Dogan, Nature (London) **395**, 580 (1998).
[6] J. M. Tranquada, B. J. Sternlieb, J. D. Axe, Y. Nakamura, and S. Uchida, Nature (London) **375**, 561 (1995).
[7] H. A. Mook, P. Dai, and F. Dogan, Phys. Rev. Lett. **88**, 097004 (2002).
[8] J. Rossat-Mignod, L. P. Regnault, C. Vettier, P. Bourges, P. Burlet, J. Bossy, J. Y. Henry, and G. Lapertot, Physica C **185–189**, 86 (1991).
[9] H. F. Fong, B. Keimer, P. W. Anderson, D. Reznik, F. Dogan, and I. A. Aksay, Phys. Rev. Lett. **75**, 316 (1995).
[10] B. Keimer, P. Bourges, H. F. Fong, Y. Sidis, L. P. Regnault, A. Ivanov, D. L. Milius, I. A. Aksay, G. D. Gu, and N. Koshizuka, J. Phys. Chem. Solids **60**, 1007 (1999).
[11] H. He, P. Bourges, Y. Sidis, C. Ulrich, L. P. Regnault, S. Pailhes, N. S. Berzigiarova, N. N. Kolesnikov, and B. Keimer, Science **295**, 1045 (2002).
[12] C. D. Batista, G. Ortiz, and A. V. Balatsky, Phys. Rev. B **64**, 172508 (2001).
[13] F. Krüger and S. Scheidl, Phys. Rev. B **67**, 134512 (2003).
[14] D. Reznik, P. Bourges, H. F. Fong, L. P. Regnault, J. Bossy, C. Vettier, D. L. Milius, I. A. Aksay, and B. Keimer, Phys. Rev. B **53**, R14 741 (1996).
[15] G. A. Samara, W. F. Hammetter, and E. L. Venturini, Phys. Rev. B **41**, 8974 (1990).
[16] E. Manousakis, Rev. Mod. Phys. **63**, 1 (1991).
[17] H. A. Mook, P. Dai, F. Dŏgan, and R. S. Hunt, Nature (London) **404**, 729 (2000).
[18] C. Stock, W. J. L. Buyers, Z. Tun, R. Liang, D. Peets, D. Bonn, W. N. Hardy, and L. Taillefer, Phys. Rev. B **66**, 024505 (2000).
[19] C. Stock, W. J. L. Buyers, R. Liang, D. Peets, Z. Tun, D. Bonn, W. N. Hardy, and R. J. Birgeneau, Phys. Rev. B **69**, 014502 (2004).
[20] P. Dai, H. A. Mook, and F. Dogan, Phys. Rev. Lett. **80**, 1738 (1998).
[21] P. Dai, H. A. Mook, S. M. Hayden, G. Aeppli, T. G. Perring, R. D. Hunt, and F. Dogan, Science **284**, 1344 (1999).
[22] P. Bourges, Y. Sidis, H. F. Fong, L. P. Regnault, J. Bossy, A. Ivanov, and B. Keimer, Science **288**, 1234 (2000).
[23] P. Dai, H. A. Mook, R. D. Hunt, and F. Dogan, Phys. Rev. B **63**, 054525 (2001).
[24] M. Arai, T. Nishijima, Y. Endoh, T. Egami, S. Tajima, K. Tomimoto, Y. Shiohara, M. Takahashi, A. Garrett, and S. M. Bennington, Phys. Rev. Lett. **83**, 608 (1999).
[25] H. F. Fong, P. Bourges, Y. Sidis, L. P. Regnault, J. Bossy, A. Ivanov, D. L. Milius, I. A. Aksay, and B. Keimer, Phys. Rev. B **61**, 14 773 (2000).
[26] P. Bourges, H. F. Fong, L. P. Regnault, J. Bossy, C. Vettier, D. L. Milius, I. A. Aksay, and B. Keimer, Phys. Rev. B **56**, R11 439 (1997).
[27] J. Rossat-Mignod, L. P. Regnault, P. Bourges, P. Burlet, C. Vettier, and J. Y. Henry, Physica B **192**, 109 (1993).
[28] H. A. Mook, M. Yethiraj, G. Aeppli, T. E. Mason, and T. Armstrong, Phys. Rev. Lett. **70**, 3490 (1993).
[29] S. Pailhes *et al.*, Phys. Rev. Lett. **91**, 237002 (2003).